

All-*trans*-retinoic acid generation is an antidotal clearance pathway for all-*trans*-retinal in the retina^{*}

Qing-qing XIA¹, Ling-min ZHANG¹, Ying-ying ZHOU¹, Ya-lin WU^{†‡2}, Jie LI^{†‡1}

¹Central Laboratory, Department of Laboratory Medicine, Huangyan Hospital of Wenzhou Medical University, Taizhou First People's Hospital, Taizhou 318020, China

²Eye Institute of Xiamen University, Fujian Provincial Key Laboratory of Ophthalmology and Visual Science, School of Medicine, Xiamen University, Xiamen 361102, China

[†]E-mail: yalinw@xmu.edu.cn; liyjie12580@126.com

Received May 27, 2019; Revision accepted Aug. 31, 2019; Crosschecked Oct. 8, 2019

Abstract: The present study was designed to analyze the metabolites of all-*trans*-retinal (atRal) and compare the cytotoxicity of atRal versus its derivative all-*trans*-retinoic acid (atRA) in human retinal pigment epithelial (RPE) cells. We confirmed that atRA was produced in normal pig neural retina and RPE. The amount of all-*trans*-retinol (atROL) converted from atRal was about 2.7 times that of atRal-derived atRA after incubating RPE cells with 10 $\mu\text{mol/L}$ atRal for 24 h, whereas atRA in medium supernatant is more plentiful (91 vs. 29 pmol/mL), suggesting that atRA conversion facilitates elimination of excess atRal in the retina. Moreover, we found that mRNA expression of retinoic acid-specific hydroxylase CYP26b1 was dose-dependently up-regulated by atRal exposure in RPE cells, indicating that atRA inactivation may be also initiated in atRal-accumulated RPE cells. Our data show that atRA-caused viability inhibition was evidently reduced compared with the equal concentration of its precursor atRal. Excess accumulation of atRal provoked intracellular reactive oxygen species (ROS) overproduction, heme oxygenase-1 (*HO-1*) expression, and increased cleaved poly(ADP-ribose) polymerase 1 (PARP1) expression in RPE cells. In contrast, comparable dosage of atRA-induced oxidative stress was much weaker, and it could not activate apoptosis in RPE cells. These results suggest that atRA generation is an antidotal metabolism pathway for atRal in the retina. Moreover, we found that in the eyes of *ABCA4*^{-/-}*RDH8*^{-/-} mice, a mouse model with atRal accumulation in the retina, the atRA content was almost the same as that in the wild type. It is possible that atRal accumulation simultaneously and equally promotes atRA synthesis and clearance in eyes of *ABCA4*^{-/-}*RDH8*^{-/-} mice, thus inhibiting the further increase of atRA in the retina. Our present study provides further insights into atRal clearance in the retina.

Key words: All-*trans*-retinal; All-*trans*-retinoic acid; Antidotal pathway; Human retinal pigment epithelial cell; Oxidative stress

<https://doi.org/10.1631/jzus.B1900271>

CLC number: R777.1

1 Introduction

Bleaching of rhodopsin activates vision transduction and releases all-*trans*-retinal (atRal) (Fig. 1a). AtRal is an important intermediate of the visual cycle, which is a complex enzymatic pathway for retinoid metabolism and regeneration within the retina (Kiser et al., 2014; Liu et al., 2016). As atRal bears a highly reactive aldehyde, which may directly react with biological macromolecules, it can cause severe

[‡] Corresponding authors

^{*} Project supported by the Zhejiang Provincial Natural Science Foundation of China (No. LQ17H120001), the Medical Science and Technology Program of Zhejiang Province (Nos. 2016KYA195 and 2017KY714), the National Natural Science Foundation of China (No. 81801424), and the 211 Talents Training Program of Taizhou, China

 ORCID: Jie LI, <https://orcid.org/0000-0001-5463-3995>

© Zhejiang University and Springer-Verlag GmbH Germany, part of Springer Nature 2019

cytotoxicity if free atRal exceeds a certain concentration in the retina (Maeda et al., 2012). Previously reported results demonstrated that defects of transporter ABCA4 and all-*trans*-retinol dehydrogenase 8 (RDH8), both of which are indispensable factors for atRal elimination in retina, generate the *ABCA4*^{-/-}*RDH8*^{-/-} mice that assemble the typical characteristics of retinopathies in age-retinal macular degeneration (AMD) patients (Maeda A et al., 2008; Maeda T et al., 2009; Molday et al., 2009; Parker and Crouch, 2010). Recently, more and more evidences have strengthened the view that failure of free atRal clearance in the retina is closely associated with the pathogenesis of AMD (Maeda A et al., 2008; Maeda T et al., 2009; Li et al., 2015, 2016).

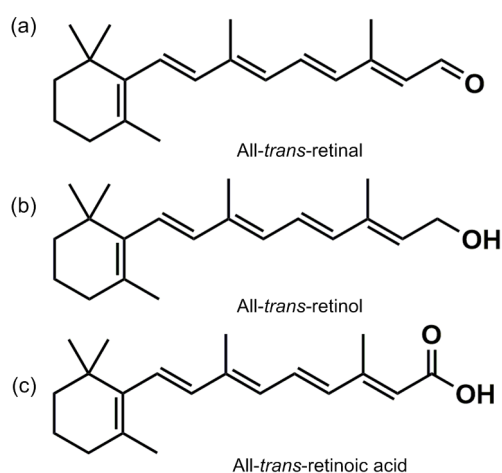


Fig. 1 Structures of all-*trans*-retinal (a), all-*trans*-retinol (b), and all-*trans*-retinoic acid (c)

Studies have shown that the concentration of rhodopsin is close to 5 mmol/L in disc membranes of the photoreceptor and 8 mmol/L in the cytoplasm of outer segments (Nickell et al., 2007). Its photo-bleaching can generate a large amount of free atRal. Accordingly, two systems were evolved for atRal elimination in the retina: one is a non-enzymatic-dependent clearance pathway, as so far no enzyme has been identified to be involved in these processes, including the synthesis of less toxic molecules like A2E, isoA2E (double bond isomer of A2E), iisoA2E (light-induced isomer of isoA2E), atRal-dimer, and other bisretinoids (Sparrow et al., 2012; Li et al., 2013; Gao et al., 2018); the other is the enzymatic-dependent pathway, for example, the reduction of atRal in the visual cycle to all-*trans*-retinol (atROL),

which is also known as vitamin A (Fig. 1b) (Chen CH et al., 2012). In addition, atRal can also be oxidized into all-*trans*-retinoic acid (atRA) (Fig. 1c) by retinaldehyde dehydrogenase (RALDH) in an irreversible reaction (Summers Rada et al., 2012; Harper et al., 2015).

As an important atRal derivative, atRA is a potent regulator of cell growth, differentiation, adhering ability, and matrix formation in various types of cells, and is indispensable for embryonic eye development (Chang et al., 2009, 2016; Duester, 2009; Du et al., 2013; Segelken et al., 2018; Todd et al., 2018). Previous research demonstrated that RALDH activity was detectable in experimental animals and postnatal human ocular tissues, including the choroid, retinal pigment epithelium (RPE), and retina (Harper et al., 2015; Summers et al., 2016). Consistently, previous results suggested that atRA was detected in the retina of guinea pigs (McFadden et al., 2004; Mao et al., 2012). However, a recent study demonstrated that atRA was absent in the eyes of atRal-accumulated *ABCA4*^{-/-}*RDH8*^{-/-} mice before or after bleaching of 40% rhodopsin (Maeda et al., 2008). Therefore, further study is required for clarification of whether atRA arises as a byproduct in the retinoid cycle.

In the retina, the RPE monolayer is critically important for maintaining normal visual transduction but is particularly vulnerable to various insults (Li et al., 2015; Hanovice et al., 2019). Thus, RPE is thought to be the primary site of pathology in AMD (Ambati and Fowler, 2012; van Lookeren Campagne et al., 2014). The disruption of atRal reduction in the neural retina may eventually result in excess atRal accumulation in RPE due to the phagocytosis of photoreceptor outer segments and free diffusion of atRal from photoreceptors (Strauss, 2005). atRal can induce massive apoptosis in RPE cells, and therefore the rapid and effective clearance of atRal from RPE cells is vital for avoiding cytotoxicity. Nevertheless, so far little is known about the metabolic processing of accumulated atRal in RPE cells. Previously reported works indicate that atRal accumulation in RPE cells generates many retinoids, including A2E, atRal-dimer, and atROL (Li et al., 2016). However, it is unclear whether atRA could be synthesized in atRal metabolism in RPE, and the role of the atRA production after atRal accumulation in the retina remains obscure.

Therefore, the present investigation aims to provide further insights into atRal clearance in the retina by analyzing atRal metabolism in vitro and measuring atRA in the eyes of the pig or *ABCA4*^{-/-}*RDH8*^{-/-} mice. We also compared the cytotoxicities of atRal and atRA, and found that the generation of atRA may significantly relieve the cytotoxicity of atRal in RPE cells.

2 Materials and methods

2.1 Reagents and cell line

AtRA (purity >98%) and atRal (purity >98%) were purchased from Aladdin (Shanghai, China) and Sigma-Aldrich (St. Louis, Missouri, USA), respectively. They were dissolved with dimethyl sulfoxide (DMSO; Sigma-Aldrich) and stored as stock solutions (20 mmol/L) in the dark at -20 °C. High-performance liquid chromatography (HPLC)-grade acetonitrile and methanol were obtained from Merck (Darmstadt, Germany). Formate (HPLC grade) was provided by Aladdin. Ammonium formate (HPLC grade) was obtained from Honeywell (Muskegon, MI, USA). Primary antibodies were mouse anti- β -actin and rabbit anti-poly(ADP-ribose) polymerase 1 (PARP1) purchased from Proteintech Company (USA).

A widely used human RPE cell line ARPE-19 that sustains the differentiated phenotype of human RPE cells was obtained from the Cell Center of Institutes of Biomedical Sciences, Fudan University (Shanghai, China). Cells were cultured in Dulbecco's modified Eagle medium (DMEM; low glucose) with 10% fetal bovine serum (Gibico, USA) and 1% (v/v) penicillin/streptomycin in a humidified incubator at 37 °C and 5% CO₂.

2.2 Analysis of cell viability

Cell viability was assayed with Cell Counting Kit-8 (CCK8; Dojindo, Japan). Briefly, after exposure of ARPE-19 cells with atRal or atRA for 6 h, 10 μ L of CCK8 was added to the medium, and incubated for 1 h at 37 °C. Then the absorbance at 490 nm in each well was spectrophotometrically measured using a microplate reader (Multiskan FC, Thermo scientific, USA). Cell viability was expressed as a proportion of control optical density.

2.3 Animals

Two pairs of *ABCA4*/*RDH8* knockout (*ABCA4*^{-/-}*RDH8*^{-/-}) mice were kindly provided by Dr. Krzysztof PALCZEWSKI (Department of Pharmacology, Case Western Reserve University, OH, USA), and were bred and raised under 12-h light/12-h dark cycle in the Laboratory Animal Center of Xiamen University (Xiamen, China). The in-cage illuminance was 60–90 lx. C57BL/6 mice purchased from Shanghai SLAC Laboratory Animal Company (Shanghai, China) were raised as the control and housed in the same circumstances. All animal procedures and experiments conformed to the requirements of the Association of Research for Vision and Ophthalmology and were approved by the Institutional Animal Care and Use Committee of Xiamen University.

2.4 Tissue extraction and ultra-performance liquid chromatography-tandem mass spectrometry (UPLC-MS/MS) analysis

Fresh pig eyes were obtained from a local abattoir. Pig RPE (1 eye/sample), pig neural retina (1 eye/sample), and murine eyes (8 months old; 8 eyes/sample) were extracted according to a previously reported method (Li et al., 2013) with some modifications. Briefly, tissues were homogenized with 1 mL ice-cold ultrapure water and 1 mL 50% methanolic chloroform in a glass tissue grinder. After centrifugation for 5 min at 3000g, the organic layer in the bottom was transferred to a 1.5-mL Eppendorf tube and dried under the Termovap sample concentrator. Tissue extraction was repeated thrice with addition of 1 mL chloroform each time. Finally, the extract was dissolved in 80% methanol and centrifuged for 5 min at 13000g. Then the supernatant was analyzed with an Acquity UPLC[®] system (Waters, USA) coupled to a triple quadrupole mass spectrometer equipped with an electrospray ionization (ESI) source (Waters, USA).

The Acquity UPLC[®] HSS C18 (1.8 μ m, 2.1 mm \times 50 mm) analytical column (Waters, USA) was maintained at 50 °C, and the temperature of the autosampler was set at 8 °C. Chromatographic conditions were optimized and achieved by a flow rate of 0.4 mL/min with mobile phases consisting of 0.1% formic acid aqueous solution (mobile phase A) and methanol with 2 mmol/L ammonium formate and

0.1% formic acid (mobile phase B). The gradient elution process was set as follows (time, % of solvent B): 0–1.0 min, 75%–86% B; 1.0–1.4 min, 86%–95% B; 1.4–2.3 min, 95% B; 2.3–2.5 min, 95%–100% B; 2.5–4.0 min, 100% B; 4.0–5.0 min, 100%–75% B; 5.0–7.0 min, 75% B.

ESI was performed in the positive ion mode. Nitrogen was used as cone and desolvation gas and argon was used as collision gas. The optimum conditions were set as follows: capillary voltage, 3.2 kV; source temperature, 150 °C; desolvation temperature, 400 °C; desolvation gas flow, 800 L/h; cone, 50 L/h. All compounds were monitored in the multiple reaction monitoring (MRM) mode for quantitative analysis. The MS collision energy, cone voltage, and dwell time were optimized for each compound (Table 1) to achieve the highest accuracy and sensitivity. The MassLynx software (Version 4.1; Waters, USA) was employed for UPLC-MS/MS data analysis and instrument control.

The quantitative ion pair was 301.22>205.00 for atRA (all-*trans*-retinoic acid-1) and 301.22>158.85 was qualitative (all-*trans*-retinoic acid-2).

2.5 Metabolisms of atRal in ARPE-19 cells

ARPE-19 cells were seeded at close to 70% confluence in a 6-well cell culture plate. Twenty-four hours later, 10 μmol/L atRal was added (2 mL), and incubated for another 24 h in the dark. Blank cells and equal volume of medium that contains 10 μmol/L atRal were used as cell control and medium control, respectively. Cells were then washed vigorously with phosphate-buffered saline (PBS) three times and harvested for intracellular metabolite extraction. Cell lysates and medium were extracted with 50% methanolic chloroform and shaken vigorously with a multi-tube vortexer. After centrifugation for 5 min at 3000g, the organic layer was transferred into a 1.5-mL Eppendorf tube and dried with a Termovap sample concentrator. Extraction was repeated thrice with addition of 0.5 mL chloroform each time. The

extract was then dissolved and centrifuged, and the supernatant was examined by an Acquity UPLC[®] system (Waters, USA) coupled to a triple quadrupole mass spectrometer (Waters, USA).

2.6 Quantitative real-time PCR (qPCR)

TRIzol reagent (Invitrogen, USA) was used for total RNA extraction and purification. RNA purity and concentration were assayed with the TGen spectrophotometer (TianGen, China). Total RNA was reversely transcribed using a ReverTra Ace[®] qPCR RT kit (Toyobo, Osaka, Japan) in accordance with the instructions. To determine the mRNA expression levels, qPCR was performed with Brilliant SYBR Green qPCR Master Mix reagent with ROX reference dye (TaKaRa, Shiga, Japan) on an ABI Prism[®] 7500 real-time PCR detection system (Applied Biosystems, USA). The $2^{-\Delta\Delta C_T}$ method was employed to quantify the relative expression level of each target gene (Livak and Schmittgen, 2001) with *GAPDH* as the internal reference. The following primer sequences in the present experiment were used: *CYP26b1*, 5'-GAC TGGGTGAAAGAGGAGTAG-3', 5'-CAGGATTAG GGATGAGCAA-3'; *HO-1*, 5'-CCAGCGGGCCAGC AACAAAGTGC-3', 5'-AAGCCTTCAGTGCCAC GGTAAGG-3' (Colombrita et al., 2003); *GAPDH*, 5'-TGACGCTGGGGCTGGCATTG-3', 5'-GGCTGG TGGTCCAGGGGTCT-3' (Li et al., 2015).

2.7 Measurement of reactive oxygen species (ROS) in RPE cells

Cellular ROS generation was detected with staining of dichloro-dihydro-fluorescein diacetate (DCFH-DA; Beyotime, Haimen, China). Briefly, cells were cultured at close to 70% confluence on 24-well culture plates. After being maintained in a cell-culture incubator for 24 h, cells were incubated with atRal or atRA for 6 h. Then the medium was discarded and 100 μL DMEM containing 1 μmol/L of DCFH-DA was added to each well. Thirty minutes later, the medium was removed and cells were washed

Table 1 ESI-MS/MS operating parameters

Analyte name	Ion transition (<i>m/z</i>)	Dwell time (s)	Cone voltage (V)	Collision energy (eV)
All- <i>trans</i> -retinol	269.16>92.97	0.03	26	22
All- <i>trans</i> -retinol- <i>d</i> ₈	277.36>98.27	0.03	26	20
All- <i>trans</i> -retinoic acid-1	301.22>205.00	0.03	22	12
All- <i>trans</i> -retinoic acid-2	301.22>158.85	0.03	22	22

ESI-MS/MS: electrospray ionization-tandem mass spectrometry

twice with PBS (37 °C). Cells were subsequently observed and photographed under a fluorescence microscope (CKX53, Olympus, Japan). Fluorescence intensities were measured with ImageJ (Version 1.4.3.67; National Institutes of Health, USA).

2.8 Western blotting

Cellular protein samples were prepared with radioimmunoprecipitation assay (RIPA) lysis buffer (Beyotime) and the protein concentration was measured with an enhanced bicinchoninic acid (BCA) protein assay kit (Beyotime). Proteins were boiled, subjected to gel electrophoresis with sodium dodecyl sulfate-polyacrylamide gel electrophoresis (SDS-PAGE) denaturing gels, and then transferred to a polyvinylidene difluoride (PVDF) membrane (Millipore, USA). After being blocked in 5% skim milk for 1 h at room temperature, the membrane was incubated with specific primary antibodies at 4 °C overnight. Then the membrane was washed with Tris-buffered saline with Tween 20 (TBST) three times, and incubated with the corresponding horseradish peroxidase-conjugated secondary antibody (Beyotime) at room temperature for 1 h. Clarity™ Western ECL substrate (Bio-Rad, USA) was used for the visualization of each protein band. All western blotting results were detected and analyzed by ChemiDox™ XRS+ with Image Lab™ software.

2.9 Statistical analysis

The results were expressed as mean±standard error of the mean (SEM). One-way analysis of variance (ANOVA), two-way ANOVA, or two-tailed unpaired Student's *t*-test was used for data analysis. $P < 0.05$ was considered statistically significant.

3 Results

3.1 Detection of atRA in pig retina

The pig retina is an excellent model for retina research as it has a similar size and anatomical architecture, cell numbers, and cell distribution to the human retina (Ruzafa et al., 2017). In the present research, fresh pig eyes were dissected and the neural retina and RPE were obtained for UPLC-MS/MS analysis. By comparison with the standard UPLC profile of atRA (retention time (t_R)=1.32 min; m/z

301.22>205.00) (Fig. 2a), we found that atRA was readily detected in the neural retina (t_R =1.34 min) and RPE (t_R =1.32 min) (Figs. 2b and 2c). Quantitative analysis showed that atRA content in the neural retina was (173.01±17.45) pmol/eye, whereas in RPE there was (64.65±13.99) pmol/eye (Figs. 2b–2d). Our data suggest that atRA may be a normal metabolite in the neural retina and RPE.

3.2 Metabolism of atRal in RPE cells

atRal (10 μmol/L) was incubated with ARPE-19 cells in the dark for 24 h. Then the cells were harvested and its hydrophobic extract was analyzed by UPLC-MS/MS. Compared to the standard UPLC profile of atROL (t_R =1.31 min; m/z 269.16>92.97) and atRA (t_R =1.34 min; m/z 301.22>205.00) (Figs. 3a and 3d), we found that no endogenous atROL or atRA existed in ARPE-19 cells (Figs. 3b and 3e). Analysis of RPE cell extract showed that atROL (t_R =1.31 min) and atRA (t_R =1.33 min) were produced after atRal incubation (Figs. 3b and 3e), and the concentrations were (1561.25±70.61) and (484.29±38.70) pmol/μg protein, respectively (Fig. 3g). We also measured retinoids in the cell culture medium supernatants. As depicted in Figs. 3c and 3f, atROL and atRA were easily detected after atRal incubation for 24 h, and their concentrations were (29.07±1.37) and (91.14±8.78) pmol/mL, respectively (Fig. 3h). No retinoids were detected in the control cell medium (RPE cell medium supernatants), but there were traces of atRA found in the medium control (medium+atRal) (Figs. 3c and 3f). It seems that atRA is more easily released into the medium while atROL exhibits a trend to accumulate within the cell (Figs. 3g and 3h). The whole culture system generated about a total of 580 pmol atRA, while atROL was about 1590 pmol, nearly 2.7 times the amount of atRA.

To further understand the generation of atRA in atRal-deposited RPE cells, we detected the expression levels of CYP26a1 and CYP26b1, which regulate retinoic acid concentration by functioning as hydroxylases specifically inactivating retinoic acid to its hydroxylated forms (Zhang et al., 2010; Ocaya et al., 2011; Parekh et al., 2019). As shown in our results (Fig. 3i), CYP26b1 was dose-dependently up-regulated by atRal-exposure in RPE cells. However, mRNA expression of CYP26a1 was undetectable (data not shown).

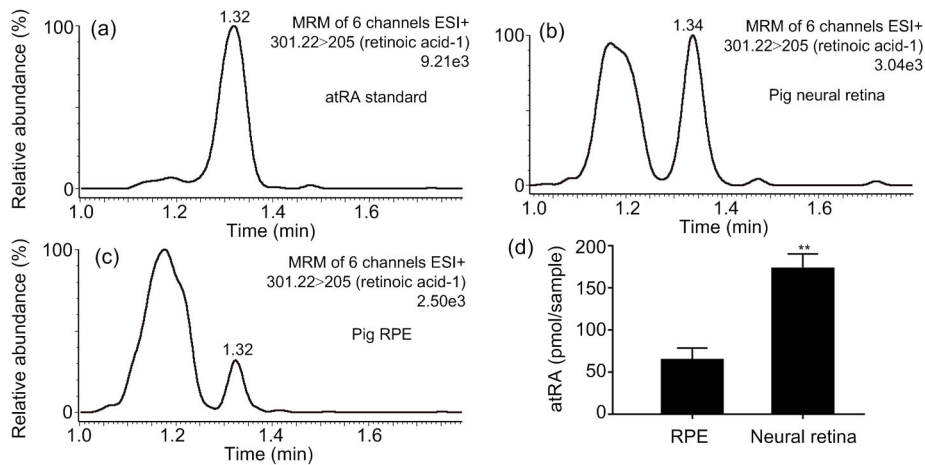


Fig. 2 Detection of atRA in pig eyes

Fresh pig eyes were dissected and the retina and RPE were obtained for UPLC-MS/MS analysis. Representative multiple reaction monitoring (MRM) spectrum of atRA was obtained from: (a) atRA standard; (b) pig neural retina; (c) pig RPE. (d) Quantitative analysis of atRA content in neural retina and RPE. Each value represents mean±standard error of the mean (SEM), $n=3$. ** $P<0.01$ vs. RPE

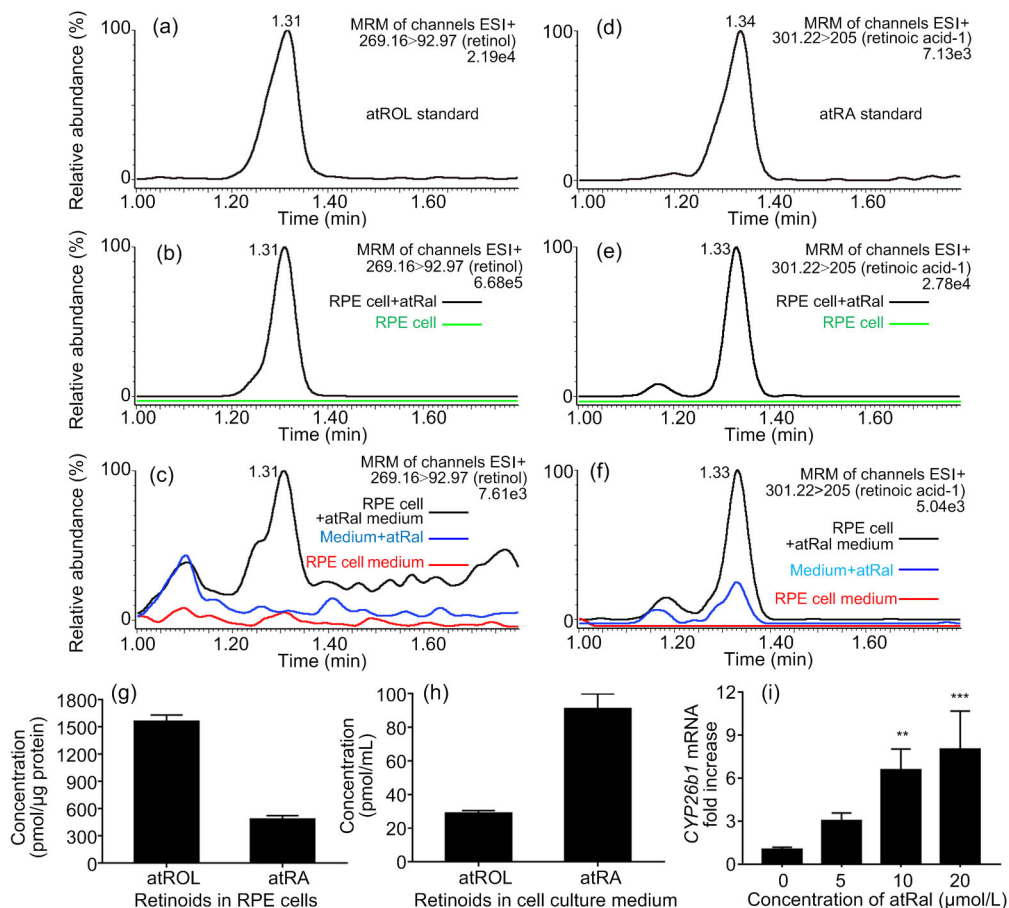


Fig. 3 Metabolism of atRA in RPE cells

RPE cells were harvested after incubation with 10 $\mu\text{mol/L}$ atRA for 24 h. Representative MRM spectra of atROL and atRA were obtained from: (a, d) atROL and atRA standards; (b, e) cell culture medium supernatants; (c, f) RPE cells extracts. (g, h) UPLC-MS/MS quantifications of atROL or atRA in atRA-treated RPE cells or the culture medium. Each value represents mean±standard error of the mean (SEM), $n=3$. (i) Six hours after atRA (0, 5, 10, and 20 $\mu\text{mol/L}$) exposure in RPE cells, the mRNA expression level of *CYP26b1* was quantified by qPCR. Each value represents mean±SEM ($n=5$ or 6), ** $P<0.01$, *** $P<0.001$ vs. 0 $\mu\text{mol/L}$ atRA

3.3 Cytotoxicities of atRA and atRal in RPE cells

Cytotoxicities of atRal or atRA in RPE cells were measured by CCK8 assay. After cells were incubated with atRal or atRA (0, 5, 10, 15, and 20 $\mu\text{mol/L}$) for 6 h, a concentration-dependent cytotoxicity was observed (Fig. 4a). However, compared to atRal treatments, cell viabilities were significantly increased in atRA-treated groups (Fig. 4a). Furthermore, as oxidative stress plays a pivotal role in atRal-related cell apoptosis (Maeda A et al., 2009; Chen Y et al., 2012; Li et al., 2015), we also examined the intracellular ROS generation with DCFH-DA staining after atRal or atRA treatment. Compared to the control group, atRal or atRA provoked dose-dependent ROS production after 6-h incubation (Figs. 4b and 4c). Nevertheless, the ROS fluorescence signal generated by an equal concentration of atRA treatment was remarkably decreased when compared to the atRal group (Figs. 4b and 4c). Heme oxygenase-1 (HO-1) is an important intracellular antioxidant, and can be highly inducible by oxidative stress (Li et al., 2015). qPCR analysis found that the mRNA expression

level of *HO-1* was greatly increased, approximately 57-fold, in 10 $\mu\text{mol/L}$ atRal-incubated RPE cells compared to the control, whereas only a 5-fold increase was observed in the atRA-treated group (Fig. 4d). To further investigate the toxicities of atRal and atRA, western blot analysis was employed to detect cleaved PARP1 (C-PARP1), which is a critical apoptosis-related protein. As depicted in Fig. 4e, C-PARP1 was concentration-dependently elevated after 6 h of atRal treatment, while it was undetectable in atRA-treated cells. These data indicate that atRA is less toxic than atRal in RPE cells.

3.4 atRA accumulation in *ABCA4*^{-/-}*RDH8*^{-/-} mice retina

ABCA4 and *RDH8* are essential transporter or reductase for atRal elimination and visual cycle maintenance (Maeda et al., 2008). Thus, the *ABCA4*^{-/-}*RDH8*^{-/-} mice were employed as the animal model of atRal clearance disruption in the retina (Maeda A et al., 2008, 2009). Indeed, our data showed that the relative intensity of the quantitative ion pair

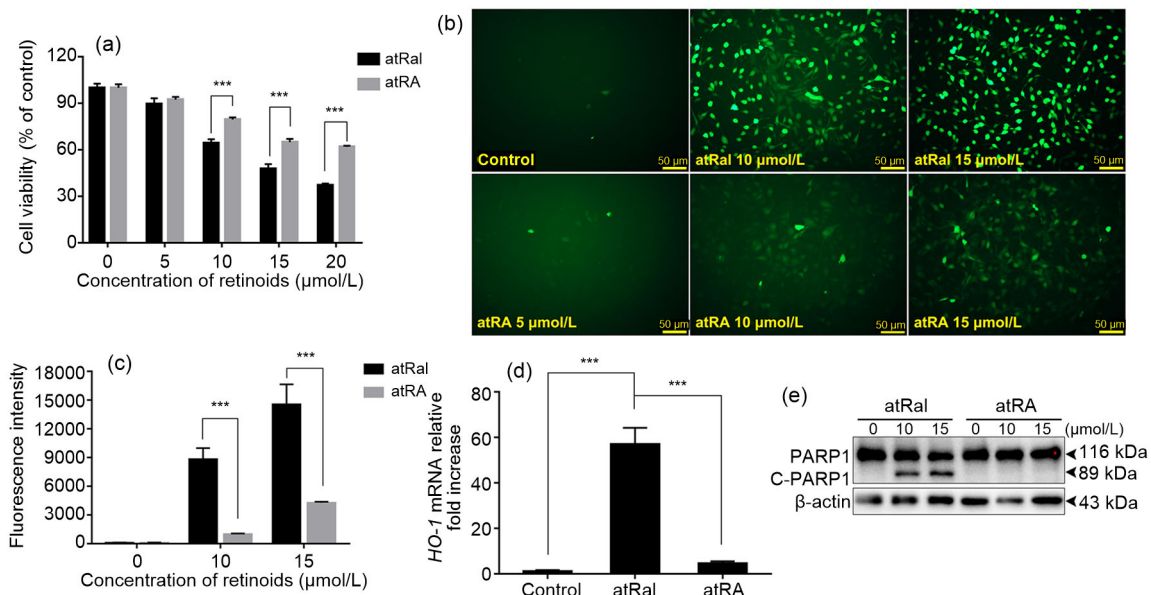


Fig. 4 Cytotoxicities of atRA and atRal in RPE cells

(a) Cell viabilities, 6 h after atRal or atRA exposure (0, 5, 10, 15, and 20 $\mu\text{mol/L}$), were evaluated by CCK8 assay. Each value represents mean \pm standard error of the mean (SEM), $n=6$. *** $P<0.001$. (b) Intracellular reactive oxygen species (ROS), 6 h after exposure of cells to atRal (10 and 15 $\mu\text{mol/L}$) or atRA (5, 10, and 15 $\mu\text{mol/L}$), were visualized by fluorescence microscopy. Scale bar=50 μm . (c) Intracellular ROS fluorescence intensities were measured with ImageJ. Each value represents mean \pm SEM ($n=3$). *** $P<0.001$. (d) Six hours after atRal or atRA (10 $\mu\text{mol/L}$) exposure in RPE cells, the mRNA expression level of heme oxygenase-1 (*HO-1*) was quantified by qPCR. Each value represents mean \pm SEM ($n=3$). *** $P<0.001$. (e) Total cell lysates, 6 h after exposure of cells to atRal or atRA (0, 10, and 15 $\mu\text{mol/L}$), were analyzed by western blot using indicated antibodies

of atROL (m/z 296.16>92.97, $t_R=1.31$ min) in $ABCA4^{-/-}RDH8^{-/-}$ mice (8 months old) was significantly decreased when compared with the control (Figs. 5a and 5b). Quantitative evaluation showed that atROL content in the control mice was about 273.56 pmol/eye. By contrast, in the eyes of $ABCA4^{-/-}RDH8^{-/-}$ mice, it was approximately 113.16 pmol/eye (Fig. 5b). However, the intensity of the atRA ion pair (m/z 301.22>205.00, $t_R=1.32$ min) in eyes of $ABCA4^{-/-}RDH8^{-/-}$ mice was not evidently different from that in the wild type (Figs. 5c and 5d). Quantitative analysis suggested that atRA was about 7.09 pmol/eye in the wild-type mice and 5.82 pmol/eye in the $ABCA4^{-/-}RDH8^{-/-}$ mice (Fig. 5d). These results suggest that delayed atRal clearance in retina significantly decreases atROL regeneration, but may not increase atRA accumulation.

4 Discussion

Free atRal released from rhodopsin following photoexcitation functions as an indispensable intermediate of the visual cycle (Liu et al., 2016). These molecules are cytotoxic and could cause retinal degeneration when excessively accumulated in the retina (Maeda A et al., 2008; Maeda T et al., 2009; Li et al., 2015). Thus, effective clearance of atRal is crucial for retinal health and vision maintenance. In the enzyme-dependent clearance pathway, the retinaldehyde

reductase activity of RDHs converts the majority of atRal into atROL (Maeda et al., 2008). Moreover, RALDH activity was also reported to be detectable in postnatal human ocular tissues (Harper et al., 2015). However, it is controversial whether atRA exists in eyes (McFadden et al., 2004; Maeda et al., 2008; Mao et al., 2012), and the role of the atRA production after atRal accumulated in the retina remains obscure.

Experimental animals, such as chicks, guinea pigs, and marmosets, are widely used in retinoid metabolism research because donated human eyes or retinal tissues are scarce. However, the size, structure, cell number, and cell distribution of retinas of these animals are far different from the human retina. Recently reported results indicated that the pig retina is an excellent experimental material for retina research as it has a similar size and anatomical architecture to the human retina (Guduric-Fuchs et al., 2009; Kim et al., 2009; Ruzafa et al., 2017). In the present study, we examined extraction of pig neural retina and RPE with UPLC-MS/MS. Our data demonstrated that atRA was detected in the pig retina (Fig. 2), approximately 173 pmol/eye in the neural retina and 64.65 pmol/eye in RPE, suggesting that the synthesis of atRA is activated in the normal neural retina and RPE.

To better understand the metabolism of atRal, the ARPE-19 cell line, which displays the morphology and functions of human RPE cells (Dunn et al., 1996), was used to simulate the excess accumulation

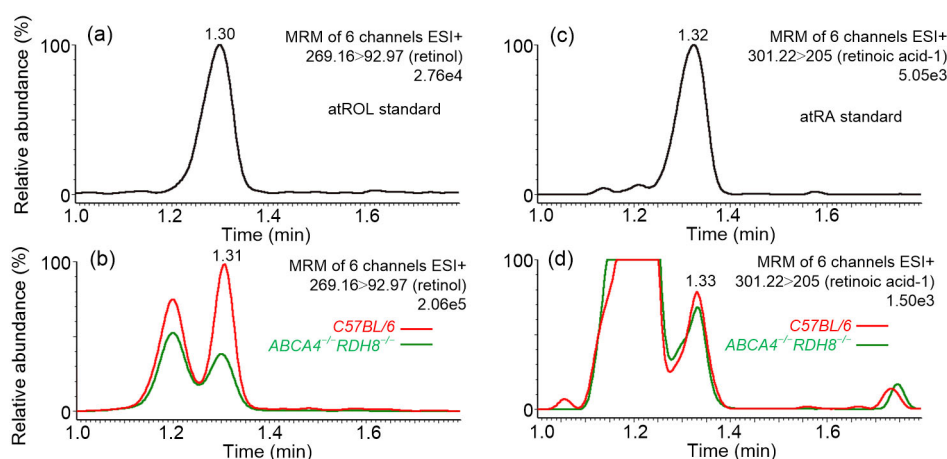


Fig. 5 atRA accumulation in eyes of $ABCA4^{-/-}RDH8^{-/-}$ mice

Representative MRM spectra of atROL were generated with: (a) atROL standard and (b) hydrophobic extracts of eyes from 8-month-old C57BL/6 (wild-type) or $ABCA4^{-/-}RDH8^{-/-}$ mice, 8 eyes/sample. Representative MRM spectra of atRA were generated with: (c) atRA standard and (d) hydrophobic extracts of eyes from 8-month-old C57BL/6 (wild-type) or $ABCA4^{-/-}RDH8^{-/-}$ mice, 8 eyes/sample

of atRal in vitro. Metabolism of atRal was further explored later. Our findings showed that atRal could be converted into atROL or atRA (Fig. 3). These actions are mainly caused by RDH activity or RALDH activity in RPE cells (Parker and Crouch, 2010; Harper et al., 2015). Concentration of atROL in RPE cells is far more than atRA (1561 vs. 484 pmol/ μ g protein), while atRA in medium supernatant is more plentiful (91 vs. 29 pmol/mL). In addition, trace amounts of atRA were also found in the medium control (medium+atRal). This may be caused by spontaneous atRal oxidization (Fig. 3f). atRA is more water-soluble, and thus it can be easily released into the medium, suggesting that atRA conversion facilitates elimination of excess atRal in the retina. On the other hand, most atROL is retained in RPE cells, so that it can be reused in the reaction of 11-*cis*-retinal regeneration in the visual cycle (Liu et al., 2016).

Studies have proven that atRA exposure can augment levels of CYP26b1, which is a hydroxylase specifically inactivating retinoic acid, and accelerate atRA metabolism (Ocaya et al., 2011). Our present results indicated that the transcription level of *CYP26b1* is significantly enhanced after atRal incubation (Fig. 3i), suggesting that atRA inactivation may be robustly proceeding in atRal-accumulated RPE cells. Moreover, as the balance between production and clearance determines the intracellular content of atRal derivative, our data also imply that the production of atRA is more than its elimination when atRal is accumulated in RPE cells.

atRA is a potent regulator of cell growth, cell differentiation, and matrix formation in various types of cells, and is thought to play an important role in the pathogenesis of myopia (Seko et al., 1998; McFadden et al., 2004; Troilo et al., 2006; Summers Rada et al., 2012; Harper et al., 2015). However, the significance of atRA generation in the atRal-accumulated retina is not fully understood. Previous studies suggest that atRal instigates ROS overproduction, and induces cell apoptosis (Li et al., 2015, 2016). Consistently, our findings elucidated that atRal accumulation could induce severe cytotoxicity (Fig. 4). Moreover, the present data showed that a certain concentration of atRA also exhibited cell viability inhibition (Fig. 4a), but the C-PARP1, which is a critical effector in the downstream of apoptosis, was undetectable (Fig. 4e), indicating that atRA accumulation in RPE cells may

result in proliferation inhibition rather than apoptosis activation. Nevertheless, its capacities for oxidative stress and cytotoxicity induction were significantly reduced when compared to the same concentration of atRal (Fig. 4). This suggests that the cytotoxicity caused by atRal was markedly mitigated by reducing oxidative stress when atRal was converted into the same concentration of atRA in RPE cells. AtRA formation may be an antidotal clearance pathway for accumulated atRal in the retina.

Due to the critical role of ABCA4 and RDH8 in the reduction of atRal into atROL, deficiencies of these two proteins will lead to excess buildup of atRal (Maeda et al., 2008). Since atROL supplementation from choroid blood vessels is very limited, atROL in the retina predominately comes from regeneration through the retinoid cycle (Liu et al., 2016). Thus, we found that the atROL level in eyes of *ABCA4*^{-/-}*RDH8*^{-/-} mice decreased significantly (Figs. 5a and 5b). Delayed elimination of atRal will augment the activation of the non-enzymatic-dependent clearance pathway, resulting in the synthesis and deposition of bisretinoids which also represent surrogate markers for aberrations in atRal clearance (Maeda A et al., 2009; Sparrow et al., 2012; Wu et al., 2013; Li et al., 2016). In addition, atRal is also converted into atRA (Figs. 5c and 5d). Though the content is small, atRA could be readily detected in the eyes of *ABCA4*^{-/-}*RDH8*^{-/-} mice (5.82 pmol/eye; Figs. 5c and 5d). However, compared to that in the wild type, atRA content in the eyes of *ABCA4*^{-/-}*RDH8*^{-/-} mice is not evidently increased (Figs. 5c and 5d). Given that the expression of atRA-specific hydroxylases, for example CYP26b1 (Fig. 3i), can be significantly elevated by atRA exposure (Ocaya et al., 2011), atRA may be easily enzymatically inactivated and eliminated in the retina. It is possible that atRal accumulation simultaneously and equally promotes atRA synthesis and clearance in eyes of *ABCA4*^{-/-}*RDH8*^{-/-} mice, thus inhibiting the further increase of atRA in the retina. This may be the reason why the atRA level is not changed in *ABCA4*^{-/-}*RDH8*^{-/-} mice when compared to that in the wild type.

Overall, our study demonstrated that atRA formation may represent as an antidotal metabolism pathway of accumulated atRal in the retina. The generation of atRA effectively attenuates the cytotoxicity of free atRal by reducing oxidative stress in RPE cells.

However, the deposition of atRA was not increased in the retina of atRal clearance aberrations, and this may be caused by the acceleration of atRA inactivation. Our present work provides us with further understanding for atRal metabolism in the retina.

Contributors

Qing-qing XIA performed the UPLC-MS/MS detection, analyzed the data, and wrote the manuscript. Ling-min ZHANG and Ying-ying ZHOU performed the cell culture, cell staining, qPCR, and western blot. Ya-lin WU and Jie LI designed the study, analyzed the data, and revised the manuscript. All authors have read and approved the final manuscript and, therefore, had full access to all the data in the study and take responsibility for the integrity and security of the data.

Compliance with ethics guidelines

Qing-qing XIA, Ling-min ZHANG, Ying-ying ZHOU, Ya-lin WU, and Jie LI declare that they have no conflict of interest.

All institutional and national guidelines for the care and use of laboratory animals were followed.

References

- Ambati J, Fowler BJ, 2012. Mechanisms of age-related macular degeneration. *Neuron*, 75(1):26-39.
<https://doi.org/10.1016/j.neuron.2012.06.018>
- Chang YC, Kao YH, Hu DN, et al., 2009. All-trans retinoic acid remodels extracellular matrix and suppresses laminin-enhanced contractility of cultured human retinal pigment epithelial cells. *Exp Eye Res*, 88(5):900-909.
<https://doi.org/10.1016/j.exer.2008.11.028>
- Chang YC, Chang YS, Hsieh MC, et al., 2016. All-trans retinoic acid suppresses the adhering ability of ARPE-19 cells via mitogen-activated protein kinase and focal adhesion kinase. *J Pharmacol Sci*, 132(4):262-270.
<https://doi.org/10.1016/j.jphs.2016.11.002>
- Chen CH, Thompson DA, Koutalos Y, 2012. Reduction of all-trans-retinal in vertebrate rod photoreceptors requires the combined action of RDH8 and RDH12. *J Biol Chem*, 287(29):24662-24670.
<https://doi.org/10.1074/jbc.M112.354514>
- Chen Y, Okano K, Maeda T, et al., 2012. Mechanism of all-trans-retinal toxicity with implications for Stargardt disease and age-related macular degeneration. *J Biol Chem*, 287(7):5059-5069.
<https://doi.org/10.1074/jbc.M111.315432>
- Colombrita C, Lombardo G, Scapagnini G, et al., 2003. Heme oxygenase-1 expression levels are cell cycle dependent. *Biochem Biophys Res Commun*, 308(4):1001-1008.
[https://doi.org/10.1016/s0006-291x\(03\)01509-2](https://doi.org/10.1016/s0006-291x(03)01509-2)
- Du YH, Hirooka K, Miyamoto O, et al., 2013. Retinoic acid suppresses the adhesion and migration of human retinal pigment epithelial cells. *Exp Eye Res*, 109:22-30.
<https://doi.org/10.1016/j.exer.2013.01.006>
- Duester G, 2009. Keeping an eye on retinoic acid signaling during eye development. *Chem Biol Interact*, 178(1-3):178-181.
<https://doi.org/10.1016/j.cbi.2008.09.004>
- Dunn KC, Aotaki-Keen AE, Putkey FR, et al., 1996. ARPE-19, a human retinal pigment epithelial cell line with differentiated properties. *Exp Eye Res*, 62(2):155-170.
<https://doi.org/10.1006/exer.1996.0020>
- Gao Z, Liao Y, Chen C, et al., 2018. Conversion of all-trans-retinal into all-trans-retinal dimer reflects an alternative metabolic/antidotal pathway of all-trans-retinal in the retina. *J Biol Chem*, 293(37):14507-14519.
<https://doi.org/10.1074/jbc.RA118.002447>
- Guduric-Fuchs J, Ringland LJ, Gu P, et al., 2009. Immunohistochemical study of pig retinal development. *Mol Vis*, 15:1915-1928.
- Hanovice NJ, Leach LL, Slater K, et al., 2019. Regeneration of the zebrafish retinal pigment epithelium after widespread genetic ablation. *PLoS Genet*, 15(1):e1007939.
<https://doi.org/10.1371/journal.pgen.1007939>
- Harper AR, Wiechmann AF, Moiseyev G, et al., 2015. Identification of active retinaldehyde dehydrogenase isoforms in the postnatal human eye. *PLoS ONE*, 10(3):e0122008.
<https://doi.org/10.1371/journal.pone.0122008>
- Kim J, Moon C, Ahn M, et al., 2009. Immunohistochemical localization of galectin-3 in the pig retina during postnatal development. *Mol Vis*, 15:1971-1976.
- Kiser PD, Golczak M, Palczewski K, 2014. Chemistry of the retinoid (visual) cycle. *Chem Rev*, 114(1):194-232.
<https://doi.org/10.1021/cr400107q>
- Li J, Yao K, Yu XN, et al., 2013. Identification of a novel lipofuscin pigment (iisoA2E) in retina and its effects in the retinal pigment epithelial cells. *J Biol Chem*, 288(50):35671-35682.
<https://doi.org/10.1074/jbc.M113.511386>
- Li J, Cai XH, Xia QQ, et al., 2015. Involvement of endoplasmic reticulum stress in all-trans-retinal-induced retinal pigment epithelium degeneration. *Toxicol Sci*, 143(1):196-208.
<https://doi.org/10.1093/toxsci/kfu223>
- Li J, Zhang YL, Cai XH, et al., 2016. All-trans-retinal dimer formation alleviates the cytotoxicity of all-trans-retinal in human retinal pigment epithelial cells. *Toxicology*, 371:41-48.
<https://doi.org/10.1016/j.tox.2016.10.005>
- Liu X, Chen JM, Liu Z, et al., 2016. Potential therapeutic agents against retinal diseases caused by aberrant metabolism of retinoids. *Invest Ophthalmol Vis Sci*, 57(3):1017-1030.
<https://doi.org/10.1167/iovs.15-18429>
- Livak KJ, Schmittgen TD, 2001. Analysis of relative gene expression data using real-time quantitative PCR and the 2^{-ΔΔCt} method. *Methods*, 25(4):402-408.
<https://doi.org/10.1006/meth.2001.1262>
- Maeda A, Maeda T, Golczak M, et al., 2008. Retinopathy in mice induced by disrupted all-trans-retinal clearance. *J*

- Biol Chem*, 283(39):26684-26693.
<https://doi.org/10.1074/jbc.M804505200>
- Maeda A, Maeda T, Golczak M, et al., 2009. Involvement of all-*trans*-retinal in acute light-induced retinopathy of mice. *J Biol Chem*, 284(22):15173-15183.
<https://doi.org/10.1074/jbc.M900322200>
- Maeda T, Maeda A, Matosky M, et al., 2009. Evaluation of potential therapies for a mouse model of human age-related macular degeneration caused by delayed all-*trans*-retinal clearance. *Invest Ophthalmol Vis Sci*, 50(10):4917-4925.
<https://doi.org/10.1167/iovs.09-3581>
- Maeda T, Golczak M, Maeda A, 2012. Retinal photodamage mediated by all-*trans*-retinal. *Photochem Photobiol*, 88(6):1309-1319.
<https://doi.org/10.1111/j.1751-1097.2012.01143.x>
- Mao JF, Liu SZ, Dou XQ, 2012. Retinoic acid metabolic change in retina and choroid of the guinea pig with lens-induced myopia. *Int J Ophthalmol*, 5(6):670-674.
<https://doi.org/10.3980/j.issn.2222-3959.2012.06.04>
- McFadden SA, Howlett MHC, Mertz JR, 2004. Retinoic acid signals the direction of ocular elongation in the guinea pig eye. *Vision Res*, 44(7):643-653.
<https://doi.org/10.1016/j.visres.2003.11.002>
- Molday RS, Zhong M, Quazi F, 2009. The role of the photoreceptor ABC transporter ABCA4 in lipid transport and Stargardt macular degeneration. *Biochim Biophys Acta*, 1791(7):573-583.
<https://doi.org/10.1016/j.bbali.2009.02.004>
- Nickell S, Park PSH, Baumeister W, et al., 2007. Three-dimensional architecture of murine rod outer segments determined by cryoelectron tomography. *J Cell Biol*, 177(5):917-925.
<https://doi.org/10.1083/jcb.200612010>
- Ocaya PA, Elmabsout AA, Olofsson PS, et al., 2011. CYP26B1 plays a major role in the regulation of all-*trans*-retinoic acid metabolism and signaling in human aortic smooth muscle cells. *J Vasc Res*, 48(1):23-30.
<https://doi.org/10.1159/000317397>
- Parekh PA, Garcia TX, Waheeb R, et al., 2019. Undifferentiated spermatogonia regulate CYP26B1 expression through NOTCH signaling and drive germ cell differentiation. *FASEB J*, 33(7):8423-8435.
<https://doi.org/10.1096/fj.201802361R>
- Parker RO, Crouch RK, 2010. Retinol dehydrogenases (RDHs) in the visual cycle. *Exp Eye Res*, 91(6):788-792.
<https://doi.org/10.1016/j.exer.2010.08.013>
- Ruzafa N, Rey-Santano C, Mielgo V, et al., 2017. Effect of hypoxia on the retina and superior colliculus of neonatal pigs. *PLoS ONE*, 12(4):e0175301.
<https://doi.org/10.1371/journal.pone.0175301>
- Segelken J, Wallisch M, Schultz K, et al., 2018. Synthesis and evaluation of two novel all-*trans*-retinoic acid conjugates: biocompatible and functional tools for retina research. *ACS Chem Neurosci*, 9(4):858-867.
<https://doi.org/10.1021/acchemneuro.7b00452>
- Seko Y, Shimizu M, Tokoro T, 1998. Retinoic acid increases in the retina of the chick with form deprivation myopia. *Ophthalmic Res*, 30(6):361-367.
<https://doi.org/10.1159/000055496>
- Sparrow JR, Gregory-Roberts E, Yamamoto K, et al., 2012. The bisretinoids of retinal pigment epithelium. *Prog Retin Eye Res*, 31(2):121-135.
<https://doi.org/10.1016/j.preteyeres.2011.12.001>
- Strauss O, 2005. The retinal pigment epithelium in visual function. *Physiol Rev*, 85(3):845-881.
<https://doi.org/10.1152/physrev.00021.2004>
- Summers JA, Harper AR, Feasley CL, et al., 2016. Identification of apolipoprotein A-I as a retinoic acid-binding protein in the eye. *J Biol Chem*, 291(36):18991-19005.
<https://doi.org/10.1074/jbc.M116.725523>
- Summers Rada JA, Hollaway LR, Lam W, et al., 2012. Identification of RALDH2 as a visually regulated retinoic acid synthesizing enzyme in the chick choroid. *Invest Ophthalmol Vis Sci*, 53(3):1649-1662.
<https://doi.org/10.1167/iovs.11-8444>
- Todd L, Suarez L, Quinn C, et al., 2018. Retinoic acid-signaling regulates the proliferative and neurogenic capacity of Müller glia-derived progenitor cells in the avian retina. *Stem Cells*, 36(3):392-405.
<https://doi.org/10.1002/stem.2742>
- Troilo D, Nickla DL, Mertz JR, et al., 2006. Change in the synthesis rates of ocular retinoic acid and scleral glycosaminoglycan during experimentally altered eye growth in marmosets. *Invest Ophthalmol Vis Sci*, 47(5):1768-1777.
<https://doi.org/10.1167/iovs.05-0298>
- van Lookeren Campagne M, LeCouter J, Yaspan BL, et al., 2014. Mechanisms of age-related macular degeneration and therapeutic opportunities. *J Pathol*, 232(2):151-164.
<https://doi.org/10.1002/path.4266>
- Wu YL, Li J, Yao K, 2013. Structures and biogenetic analysis of lipofuscin bis-retinoids. *J Zhejiang Univ-Sci B (Biomed & Biotechnol)*, 14(9):763-773.
<https://doi.org/10.1631/jzus.B1300051>
- Zhang Y, Zolfaghari R, Ross AC, 2010. Multiple retinoic acid response elements cooperate to enhance the inducibility of CYP26A1 gene expression in liver. *Gene*, 464(1-2):32-43.
<https://doi.org/10.1016/j.gene.2010.05.004>

中文概要

题目: 全反式维甲酸的生成是视网膜中全反式视黄醛的一种解毒代谢途径

目的: 探讨视网膜中全反式视黄醛 (atRal) 能否代谢生成全反式维甲酸 (atRA), 并比较两者对视网膜色素上皮细胞 (RPE) 的细胞毒性作用, 以阐明 atRA 生成的意义。

创新点: 建立 atRA 的超高效液相串联质谱 (UPLC-MS/MS) 检测方法, 并证明 atRA 的生成是视网膜中 atRal 的重要解毒代谢通路。

方法: 利用 UPLC-MS/MS 分别检测猪眼神视网膜及 RPE 层中 atRA 的含量; 利用 ARPE-19 细胞系模拟 atRal 在 RPE 中累积, 用 UPLC-MS/MS 检测细胞内及培养基中 atRA 的含量, 并用定量聚合酶链反应 (qPCR) 检测 CYP26b1 的表达; 利用 CCK8、DCFH-DA 染色、qPCR、western blot 等方法对比等浓度 atRA 和 atRal 在 RPE 细胞中所诱

导的细胞毒性、氧化应激、凋亡相关蛋白表达水平; 用 UPLC-MS/MS 检测视网膜 atRal 清除障碍的 *ABCA4^{-/-}RDH8^{-/-}* 小鼠眼球中 atRA 及全反式视黄醇。

结论: 明确 atRA 在正常视网膜中能够代谢产生; 证明其形成有利于 RPE 细胞中累积的 atRal 迅速代谢消除; 其自身诱导细胞氧化应激的能力显著低于 atRal, 因而能显著减弱后者的细胞毒性。

关键词: 全反式维甲酸; 全反式视黄醛; 解毒途径; 视网膜色素上皮细胞; 氧化应激